Fabrication of As-doped n-type $BaSi_2$ epitaxial films grown by molecular beam epitaxy

Sho Aonuki, Yudai Yamashita, Kaoru Toko, and Takashi Suemasu

Institute of Applied Physics, University of Tsukuba, Ibaraki 305-8573, Japan

We grow As-doped $BaSi_2$ epitaxial films by molecular beam epitaxy (MBE) with GaAs granules as an As source and investigated their electrical and optical properties by changing a substrate temperature (T_S) and a crucible temperature of GaAs (T_{GaAs}) during MBE. Secondary ion mass spectrometry revealed that the density of As atoms in $BaSi_2$ films was surely changed by T_{GaAs}. The full width at half-maximum evaluated by the x-ray ω-scan rocking curve measurement reached a minimum of 0.36 ° at T_S = 600 °C. We investigated the T_S dependence of electron concentration (n) and mobility by Hall measurement. n increased with decreasing T_S and reached a maximum of 4.3×10^{18} cm^{-3}. The photoresponsivity of the As-doped $BaSi_2$ films was higher than that of undoped ones at the same bias voltage, probably thanks to the reduction of point defects by As doping.

1. Introduction

Barium silicide ($BaSi_2$) has been attracting considerable attention as a new candidate for thin film solar cell materials.[1)] $BaSi_2$ consists of Si and Ba, which are abundant elements in the earth's crust, and the band gap of $BaSi_2$ (1.3 eV) is suitable for solar cell applications.[2–4)] Moreover, a large absorption coefficient (3×10^4 cm^{-1} at 1.5 eV) exceeding those of $Cu(In,Ga)(Se,S)_2$ is compatible with an ample minority carrier lifetime (> 10 μs).[5,6)] Very recently, we achieved the conversion efficiency of 9.9% in p^+-$BaSi_2$/n-Si heterojunction solar cells.[7–9)] In addition, the operation of a $BaSi_2$ homojunction solar cell was demonstrated on a p-Si(111) substrate.[10,11)] In this structure, an antimony (Sb)-doped n-$BaSi_2$ layer[12)] was used for the topmost layer. This is because a low-temperature-grown Sb-doped n-$BaSi_2$ layer is suitable only to the topmost layer since the diffusion coefficient of Sb in $BaSi_2$ is very large.[13)] However, the following problem arises when the layered structure is n-$BaSi_2$/p-$BaSi_2$/p-Si. Due to a small electron affinity of $BaSi_2$ (0.32 eV),[14)] there is a large conduction band offset of approximately 0.8 eV and a large valence band offset of approximately 0.6 eV at $BaSi_2$/Si heterointerfaces when a Si substrate is adopted.[15)] Therefore, the flow of photogenerated carriers is blocked by these band offsets at the p-$BaSi_2$/p-Si interface as shown in Fig. 1(a). It is therefore necessary to form a p^+-$BaSi_2$/p^+-Si tunnel junction when a p-type Si substrate is used. However, the crystallinity of p^+-$BaSi_2$ films grown on a low-resistivity (ρ) p^+-Si substrate degrades,[16)] leading to the decrease of shunt resistance and thereby much smaller efficiencies than expected.[17)] In this study, we propose an alternative structure, that is a $BaSi_2$ homojunction solar cell on an n-Si substrate as shown in Fig. 1(b). In this structure, a tunnel junction is not necessary since the flow of photogenerated carriers is not blocked at the n-$BaSi_2$/n-Si heterointerface. To realize this structure, it is indispensable to explore n-$BaSi_2$ films doped with impurities other than Sb.

The valence band maximum of $BaSi_2$ is composed mainly of Si 3s and 3p orbitals and it is reported that Si atoms are more easily substituted than Ba atoms in the lattice.[2,18)] Therefore, substitution of Si atoms with group 15 elements such as Sb, arsenic (As), and phosphorous (P) increases the valence electron concentration,[11,19,20)] and therefore n-type $BaSi_2$ forms. Regarding As-doped $BaSi_2$ and P-doped $BaSi_2$, the n-type conductivity was reported by ion implantation;[19,20)] however, the electron concentration n does not exceed 10^{18} cm^{-3} in P-doped $BaSi_2$ films by molecular beam epitaxy (MBE).[21)] On the other hand, there has been no report thus far on As-doped n-$BaSi_2$ grown by MBE. We should also note that the diffusion coefficient

of As atoms in $BaSi_2$ films is much smaller than those of Sb.[12] In this work, we thereby aim to fabricate As-doped n-$BaSi_2$ epitaxial films grown by MBE and evaluate their electrical and optical properties. We employed GaAs granules as a source of As rather than elemental As. As atoms are supplied in the form of As_2 from GaAs granules, whereas As_4 molecules are supplied from elemental As sources.[22] According to ref. 23, As_2 is more easily decomposed into As atoms than As_4, enabling us to substitute some of Si atoms with As atoms in the $BaSi_2$ lattice more efficiently. We can neglect the doping effect of Ga atoms. This is because the vapor pressure of Ga is much smaller than that of As_2.[23]

2. Experiment method

As-doped Si and $BaSi_2$ epitaxial films were formed on p-Si(111) substrates by MBE equipped with an electron-beam gun for Si and Knudsen cells for Ba and GaAs. For Hall measurement, high-resistivity (ρ > 1000 Ωcm) p-Si(111) substrates were used. In contrast, low-ρ (< 0.01 Ωcm) n^+-Si(111) substrates were used for photoresponsivity measurement. The fabrication procedure of As-doped Si films is as follows. After thermal cleaning (TC) of the Si substrate by heating at 900 °C for 30 min in ultrahigh vacuum, As-doped Si films were grown at a fixed substrate temperature T_S = 600 °C by MBE. The thickness of As-doped Si films was approximately 150 nm. The crucible temperature of GaAs was set at T_{GaAs} = 550, 650, and 750 °C. Finally, a 3-nm-thick amorphous Si (a-Si) capping layer was formed *in situ* at T_S = 180 °C. 1-mm-diameter Al electrodes with a thickness of 150 nm were deposited by sputtering.

We next grew As-doped $BaSi_2$ epitaxial films as follows. After TC, a few-nm-thick $BaSi_2$ template layer was formed by reactive deposition epitaxy, in which only Ba was supplied on a heated Si substrate. This layer works as a seed crystal for overlayers.[24] After that, As-doped $BaSi_2$ films were formed by MBE at various values of T_{GaAs} and T_S.[25, 26] First, T_{GaAs} was varied in the range 250 – 450 °C while T_S was fixed at 600 °C. As described later, however, we were not able to control n by changing T_{GaAs}. Therefore, we next set T_{GaAs} at 350 °C and varied T_S in the range 500 – 700 °C. For photoresponsivity measurement, T_{GaAs} was changed from 250 to 450 °C with keeping T_S constant at 600 °C. The thickness of As-doped $BaSi_2$ films was approximately 500 nm. Then, a 3-nm-thick a-Si capping layer was formed for surface passivation.[27] The bond configuration changes abruptly at the $BaSi_2$ surface. According to an analysis of the surface structure of $BaSi_2$ epitaxial layers using coaxial-collision ion scattering

spectroscopy conducted by Katayama *et al*., an *a*-axis-oriented $BaSi_2$ epitaxial films is terminated by Si_4 tetrahedra.[28,29] Therefore, surfaces may contain very high densities of trap states in the band gap.[30] Such surface defects deteriorate solar cell performance because short-wavelength light is absorbed close to the surface. Therefore, surface passivation is very important for materials like $BaSi_2$ that possess large absorption coefficients. Finally, 1-mm-diameter ITO electrodes with the thickness of 80 nm on the surface and Al electrodes with the thickness of 150 nm on the whole back side were formed by sputtering.

Crystalline quality of grown films was characterized by θ-2θ X-ray diffraction (XRD; Rigaku Smart Lab) using Cu Kα radiation, and reflection high-energy electron diffraction (RHEED). Depth profiles of As atoms were evaluated by secondary ion mass spectrometry (SIMS) with Cs^+ ions. Hall measurement was performed with Van der Pauw method.[31] Photoresponse spectra were collected at a bias voltage (V_{bias}) of −0.5 V applied to the front ITO electrode with respect to the backside Al electrode by a lock-in technique using a xenon lamp (Bunko Keiki, SM-1700A) and a single monochromator with a focal length of 25 cm (Bunko Keiki, RU-60N). The light intensity of the lamp was calibrated using a pyroelectric sensor (Melles Griot, 13PEM001/J). All the measurement was performed at room temperature.

3. Results and discussion

Figure 2 shows the T_{GaAs} dependences of n and mobility μ of As-doped Si films. T_S was fixed at 600 °C. Hall measurement revealed that n increased with T_{GaAs}, and n reached a maximum of 3.7×10^{18} cm^{-3} at T_{GaAs} = 750 °C. The μ decreased accordingly. This result was in agreement with those reported on As-doped n-Si films by using GaAs as a source of As.[32]

After confirming the formation of n-Si films by heating GaAs granules, we next move on to As-doped $BaSi_2$ films. First, we checked the presence of As atoms in the grown films by SIMS. Figure 3(a) and 3(b) show the depth profiles of As atoms in As-doped $BaSi_2$ films and secondary ion intensity of Ba + Si in As-doped $BaSi_2$ films grown at T_{GaAs} = 350 and 750 °C, respectively. T_S was set at 600 and 650 °C, respectively. Please note that the measured As concentration (N_{As}) was not corrected because reference samples with a controlled number of As atoms doped in $BaSi_2$ films have not yet been prepared. In this work, we employed As-doped Si as a reference. N_{As} was approximately 3×10^{18} cm^{-3} in Fig. 3(a) and approximately 10^{22} cm^{-3} in

Fig. 3(b). The limit of detection by SIMS is approximately 4×10^{17} cm^{-3}. There results mean that the N_{As} changes by T_{GaAs} in $BaSi_2$ films.

Figure 4(a) shows the θ-2θ XRD patterns and RHEED patterns observed along the Si[11-2] azimuth after the growth of As-doped $BaSi_2$ films. T_S was varied in the range 500 – 700 °C, while T_{GaAs} was fixed at 350 °C. In all the samples, the diffraction peaks corresponding to *a*-axis-oriented $BaSi_2$ films were detected. Therefore, *a*-axis-oriented As-doped $BaSi_2$ films was grown regardless of T_S. In the sample grown at T_S = 500 °C, however, streaky RHEED pattern was not obtained. In contrast, for samples grown at 550 °C ≤ T_S ≤ 700 °C, streaky RHEED patterns were observed. On the basis of these results, we can state that *a*-axis-oriented As-doped $BaSi_2$ films were grown epitaxially in the range of T_S = 550 – 700 °C. To find the optimum T_S among them, we evaluated the T_S dependence of the full width at half-maximum (FWHM) of $BaSi_2$ 600 peak by ω-scan x-ray rocking curve measurement. The result is presented in Fig. 4(b). The FWHM decreased with T_S, reached a minimum of 0.36 ° at T_S = 600 °C, and increased for higher T_S, suggesting that the optimum T_S was 600 °C from the viewpoint of crystalline quality. Similar tendency of FWHM values against T_S was reported for undoped $BaSi_2$ films.[33)]

We therefore set T_S at 600 °C and changed T_{GaAs} from 250 to 450 °C to form As-doped n-$BaSi_2$ films. In contrast to our prediction, however, we could not control *n* by changing T_{GaAs} at T_S = 600 °C. Figure 3(a) shows the presence of As atoms in the $BaSi_2$ films grown at T_S = 600 °C and T_{GaAs} = 350°C. The increase of T_{GaAs} increases the concentration of As atoms in the $BaSi_2$ films. Therefore, the fact that the *n* of As-doped $BaSi_2$ films cannot be controlled by T_{GaAs} means that doped As atoms did not occupy the Si sites in the lattice of $BaSi_2$. Similar results were obtained in Sb-doped $BaSi_2$ films in ref. 12. Thereby, we next fixed T_{GaAs} at 350 °C and varied T_S from 500 to 700 °C for As-doped $BaSi_2$ films. Figure 5 shows the T_S dependence of *n* and μ of As-doped $BaSi_2$ films. *n* increased with decreasing T_S, and reached 4.3×10^{18} cm^{-3} at T_S = 550 °C. This value of *n* is acceptable for the bottom layer of a $BaSi_2$ homojunction solar cell. *n* decreased sharply when T_S was 600 °C and over. This result shows that the value of *n* can be controlled by T_S. The value of μ decreased with increasing T_S. As shown in Fig. 4(b), the crystalline quality of $BaSi_2$ films degraded for samples grown at T_S > 600 °C. We therefore attribute such reduction of μ partly to the degradation of crystalline quality of As-doped $BaSi_2$ films.

Figure 6 shows the photoresponse spectra of As-doped $BaSi_2$ films grown with T_{GaAs} = 250 – 450 °C. T_S was fixed at 600 °C. A V_{bias} of −0.5 V was applied to the front ITO electrode with respect to the backside Al electrode. Photoresponsivity was increased with T_{GaAs}, and reached a maximum of approximately 0.8 A/W at a wavelength of 800 nm for sample grown at T_{GaAs} = 350 °C. The obtained photoresponsivity was higher than that of undoped $BaSi_2$ films at the same value of V_{bias}.[34)] We attribute this improvement of photoresponsivity to the reduction of point defects in As-doped $BaSi_2$ films. In undoped $BaSi_2$ films, photoresponsivity and carrier lifetime were improved significantly by hydrogen (H) passivation.[35)] H atoms in $BaSi_2$ films are considered to inactivate Si vacancies, which are most likely to form in $BaSi_2$.[36)] Likewise, we speculate that inactivation of Si vacancies by doping As atoms in As-doped $BaSi_2$ films occurs. The photoresponsivity is proportional of the ratio of carrier lifetime to carrier transit time,[37)] meaning that the reduction of carrier mobility decreases the photoresponsivity. As shown in Fig. 5, the electron mobility of As-doped $BaSi_2$ films decreases with T_S. This is caused by the degradation of crystalline quality of As-doped $BaSi_2$ films as shown in Fig. 4(b), suggesting that the mobility of photogenerated holes also decreases with T_S. Therefore, we consider the reason why the photoresponsivity reaches a maximum at a certain value (T_{GaAs} = 350 °C) as follows. The photoresponsivity increases with T_{GaAs} because of the reduction of point defects by doped As atoms. However, further increase of As atoms degrades the crystalline quality of As-doped $BaSi_2$ films, leading to the reduction of carrier mobilities and therefore photoresponsivity.

4. Conclusion

We fabricated As-doped n-$BaSi_2$ films grown by MBE and evaluated their electrical and optical properties. Highly *a*-axis-oriented As-doped $BaSi_2$ films were grown epitaxially on Si(111) substrates. The optimum T_S of As-doped $BaSi_2$ was 600 °C in terms of crystalline quality. n increased with decreasing T_S, and reached a maximum of 4.3×10^{18} cm^{-3} at T_S = 550 °C and T_{GaAs} = 350 °C. Moreover, photoresponsivity was enhanced by As doping and the highest photoresponsivity was obtained for As-doped $BaSi_2$ films at T_S = 600 °C and T_{GaAs} = 350 °C. We ascribe the higher photoresponsivity of As-doped $BaSi_2$ films compared to undoped $BaSi_2$ films to the reduction of point defects by As doping as is the case with atomic hydrogen passivated $BaSi_2$ films.

ACKNOWLEDGEMENTS

This work was financially supported by JSPS KAKENHI Grant Numbers 17K18865 and 18H03767 and JST MIRAI. One of the authors (Y. Y.) was financially supported by Grant-in-Aid for JSPS Fellows (19J21372).

Captions of figures

Fig. 1. Schematic of band alignments and the flow of photogenerated carriers in (a) n-$BaSi_2$/p-$BaSi_2$ on p-Si and (b) p-$BaSi_2$/n-$BaSi_2$ on n-Si under illumination.

Fig. 2. T_{GaAs} dependence of n and μ of As-doped Si grown with T_{GaAs} = 550 – 750 °C. T_S is 600 °C.

Fig. 3. SIMS depth profile of N_{As} and secondary ions (Ba + Si) of $BaSi_2$ films grown with (a) T_{GaAs} = 350 °C, (b) T_{GaAs} = 750 °C. T_S is 600 °C in (a) and 650 °C in (b).

Fig. 4. (a) θ-2θ XRD and RHEED patterns of As-doped $BaSi_2$ films taken along the Si [11-2] azimuth for samples grown at T_S = 500 − 700 °C. T_{GaAs} is 350 °C, and (b) T_S dependence of FWHM values of $BaSi_2$ 600 peaks for samples grown at T_S = 500 – 700 °C, evaluated by x-ray ω-scan rocking curve measurement.

Fig. 5. T_S dependences of n and μ of As-doped $BaSi_2$ films grown with T_S of 500 − 700 °C. T_{GaAs} is 350 °C.

Fig. 6. Photoresponse spectra of As-doped $BaSi_2$ films grown with T_{GaAs} = 250 – 450 °C and T_S = 600 °C at V_{bias} = −0.5 V.

References

1) T. Suemasu, and N. Usami, J. Phys. D. Appl. Phys. **50**, 023001 (2017).
2) D. B. Migas, V. L. Shaposhnikov, and V. E. Borisenko, Phys. Status Solidi B **244**, 2611 (2007).
3) M. Kumar, N. Umezawa, and M. Imai, J. Appl. Phys. **115**, 203718 (2014).
4) M. Kumar, N. Umezawa, and M. Imai, Appl. Phys. Express **7**, 071203 (2014).
5) K. Toh, T. Saito, and T. Suemasu, Jpn. J. Appl. Phys. **50**, 068001 (2011).
6) M. Baba, K. Toh, K. Toko, N. Saito, N. Yoshizawa, K. Jiptner, T. Sekiguchi, K. O. Hara, N. Usami, and T. Suemasu, J. Cryst. Growth **348**, 75 (2012).
7) S. Yachi, R. Takabe, H. Takeuchi, K. Toko, and T. Suemasu, Appl. Phys. Lett. **109**, 072103 (2016).
8) D. Tsukahara, S. Yachi, H. Takeuchi, R. Takabe, W. Du, M. Baba, Y. Li, K. Toko, N. Usami, and T. Suemasu, Appl. Phys. Lett. **108**, 152101 (2016).
9) T. Deng, T. Sato, Z. Xu, R. Takabe, S. Yachi, Y. Yamashita, K. Toko, and T. Suemasu, Appl. Phys. Express **11**, 062301 (2018).
10) K. Kodama, R. Takabe, S. Yachi, K. Toko, and T. Suemasu, Jpn. J. Appl. Phys. **57**, 031202 (2018).
11) K. Kodama, Y. Yamashita, K. Toko, and T. Suemasu, Appl. Phys. Express **12**, 041005 (2019).
12) M. Kobayashi, Y. Matsumoto, Y. Ichikawa, D. Tsukada, and T. Suemasu, Appl. Phys. Express **1**, 051403 (2008).
13) N. Zhang, K. Nakamura, M. Baba, K. Toko, and T. Suemasu, Jpn. J. Appl. Phys. **53**, 04ER02 (2014).
14) T. Suemasu, K. Morita, M. Kobayashi, M. Saida, and M. Sasaki, Jpn. J. Appl. Phys. **45**, L519 (2006).
15) K. Kodama, R. Takabe, T. Deng, K. Toko, and T. Suemasu, Jpn. J. Appl. Phys. **57**, 050310 (2018).
16) Y. Yamashita, S. Yachi, R. Takabe, T. Sato, M. E. Bayu, K. Toko, and T. Suemasu, Jpn. J. Appl. Phys. **57**, 025501 (2018).
17) T. Suemasu, Jpn. J. Appl. Phys. **54**, 07JA01 (2015).
18) Y. Imai, and A. Watanabe, Intermetallics **15**, 1291 (2007).
19) K. O. Hara, N. Usami, M. Baba, K. Toko, and T. Suemasu, Thin Solid Films **567**, 105 (2014).
20) K. O. Hara, Y. Hoshi, N. Usami, Y. Shiraki, K. Nakamura, K. Toko, and T. Suemasu, Thin Solid Films **557**, 90 (2014).
21) R. Takabe, M. Baba, K. Nakamura, W. Du, M. A. Khan, S. Koike, K. Toko, K. O. Hara, N. Usami, and T. Suemasu, Phys. Status Solidi C **10**, 1753 (2013).
22) J. R. Arthur, J. Phys. Chem. Solids **28**, 2257 (1967).
23) C. T. Foxon, J. A. Harvey, and B. A. Joyce, J. Phys. Chem. Solids **34**, 1693 (1973).
24) Y. Inomata, T. Nakamura, T. Suemasu, and F. Hasegawa, Jpn. J. Appl. Phys. **43**, 4155 (2004).
25) Y. Inomata, T. Nakamura, T. Suemasu, and F. Hasegawa, Jpn. J. Appl. Phys. **43**, L478 (2004).
26) Y. Inomata, T. Suemasu, T. Izawa, and F. Hasegawa, Jpn. J. Appl. Phys. **43**, L771 (2004).
27) R. Takabe, K. O. Hara, M. Baba, W. Du, N. Shimada, K. Toko, N. Usami, and T. Suemasu,

J. Appl. Phys. **115**, 193510 (2014).
28) S. Okasaka, O. Kubo, D. Tamba, T. Ohashi, H. Tabata, and M. Katayama, Surf. Sci. **635**, 115 (2015).
29) O. Kubo, T. Otsuka, S. Okasaka, S. Osaka, H. Tabata, and M. Katayama, Jpn. J. Appl. Phys. **55**, 08NB11 (2016).
30) D. B. Migas, V. O. Bogorodz, A. V. Krivosheeva, V. L. Shaposhnikov, A. B. Filonov, and V. E. Borisenko, Jpn. J. Appl. Phys. **56**, 05DA03 (2017).
31) L. J. van der Pauw, Philips Res. Reports **13**, 1 (1958).
32) R. A. A. Kubiak, W. Y. Leong, and E. H. C. Parker, Appl. Phys. Lett. **46**, 565 (1985).
33) R. Takabe, K. Nakamura, M. Baba, W. Du, M. A. Khan, K. Toko, M. Sasase, K. O. Hara, N. Usami, and T. Suemasu, Jpn. J. Appl. Phys. **53**, 04ER04 (2014).
34) R. Takabe, T. Deng, K. Kodama, Y. Yamashita, T. Sato, K. Toko, and T. Suemasu, J. Appl. Phys. **123**, 045703 (2018).
35) Z. Xu, D. A. Shohonov, A. B. Filonov, K. Gotoh, T. Deng, S. Honda, K. Toko, N. Usami, D. B. Migas, V. E. Borisenko, and T. Suemasu, Phys. Rev. Mater. **3**, 065403 (2019).
36) M. Kumar, N. Umezawa, W. Zhou, and M. Imai, J. Mater. Chem. A **5**, 25293 (2017).
37) S. M. Sze, Physics of Semiconductor Devices, 2nd ed. (Wiley, New York, 1981).

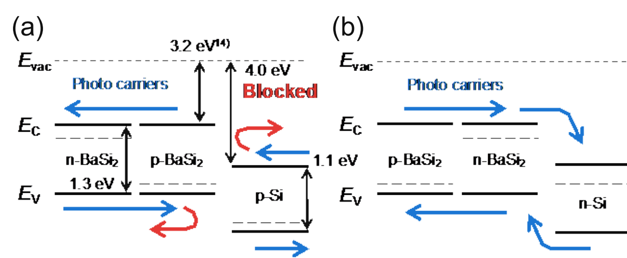

Fig. 1

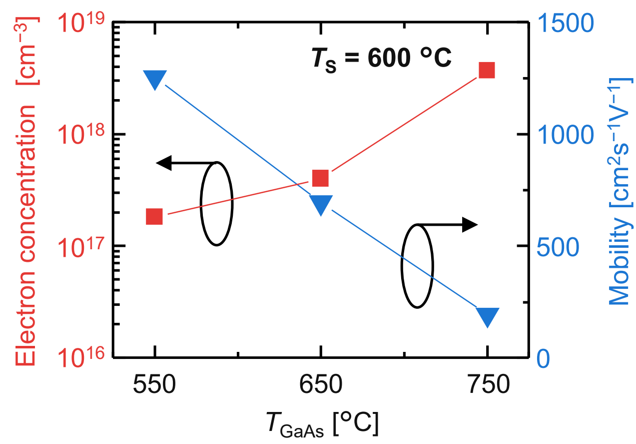

Fig. 2

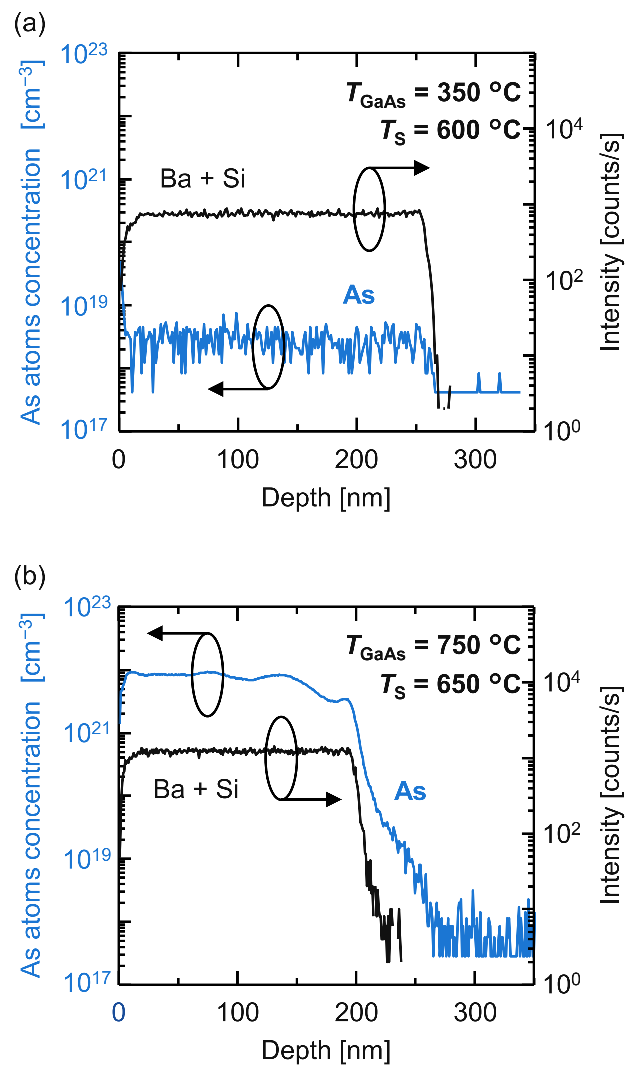

Fig. 3

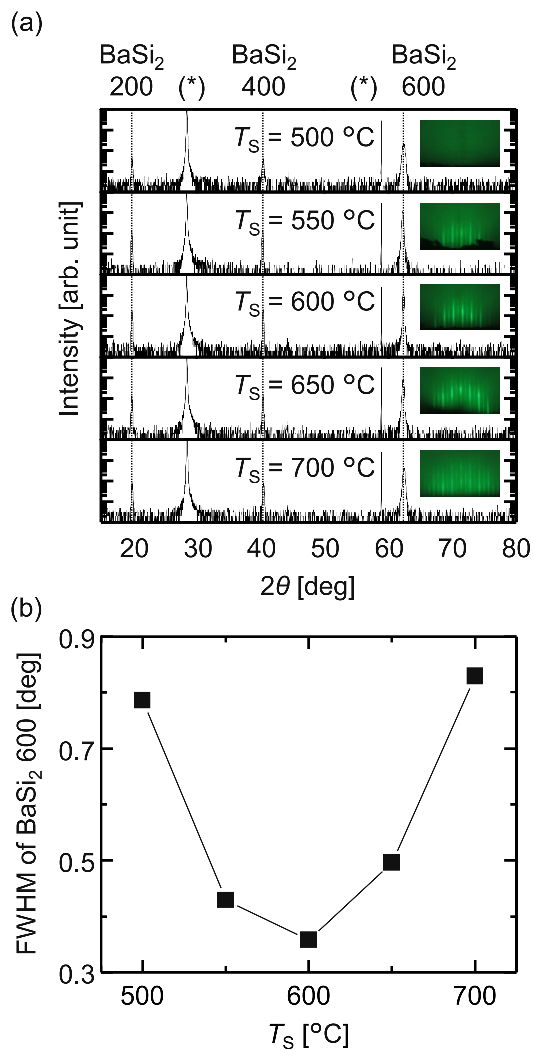

Fig. 4

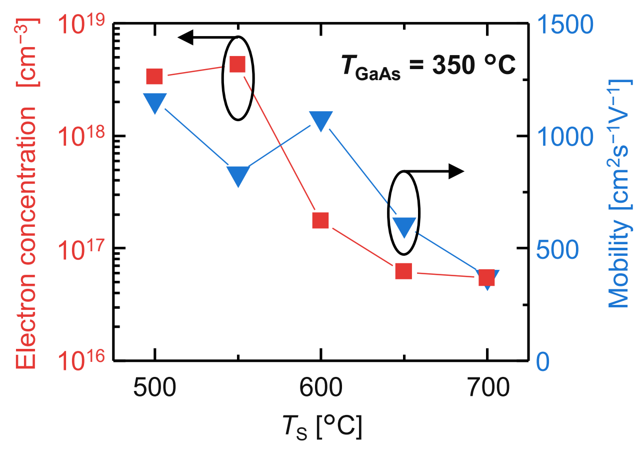

Fig.5

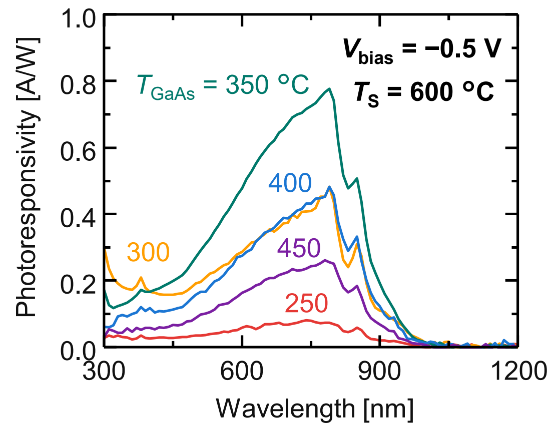

Fig. 6